Research Article

Investigation on behavior and seismic performance of reduced beam sections

İbrahim Ermeydan [1], Alirıza İlker Akgönen [2]*

[1]   Department of Civil Engineering, Kahramanmaraş Sütçü İmam University, Kahramanmaraş (Turkiye),
     ermeydanibo@gmail.com
[2]   Department of Civil Engineering, Kahramanmaraş Sütçü İmam University, Kahramanmaraş (Turkiye),
     ilkerakgonen@ksu.edu.tr
     *Correspondence: ilkerakgonen@ksu.edu.tr

Abstract: Engineers prefer reduced beam section (RBS) connections in steel moment frames built in earthquake zones due to their many benefits. The RBS shape design significantly affects joint behavior. This paper examines the effect of RBS geometry on joint behavior and seismic performance using ANSYS finite element analysis software. RBS connections are investigated using European profiles and steel grades due to the limited number of studies using European profiles in the literature. The simulation study is carried out in three stages. In the first stage, an experimental study in the literature is simulated, and the reliability of the created finite element model is checked. In the second stage, geometric changes are made to the verified numerical model, and the obtained new models are examined under monotonic loading to observe the effect of RBS geometry on moment-rotation behavior. In the third stage, the effect of the change in the RBS geometry on the seismic performance is investigated under cyclic loading. As a result of the study, the effects of various changes made in the RBS geometry on the joint behavior and seismic performance are presented graphically. By using the results of the analysis under monotonic loading, the regression analysis is carried out, and the formulas giving the elastic-plastic stiffness, elastic moment capacity, and elastic rotation angle of the support are derived. Besides, simulation models show that the RBS joints' seismic performance met the minimum criteria specified in the earthquake code (AISC/ANSI 341-16) when European steel profiles and quality are applied.

Keywords: Cycling loading, European steel shapes, moment connection, reduced beam section, steel moment resisting frame.

1.   Introduction

It is essential to provide strong column-weak beam behavior to obtain ductility and high energy dissipation in steel moment frame structures built in earthquake zones. The use of Reduced Beam Section (RBS) in moment frames is one method to achieve this behavior (Karip, 2014). RBS connections are created by cross-section reductions made at the beam's top and bottom flanges (Figure 1) near the connection zone. RBS connections divert the possible damage to the beam that may occur in the column or connection zone due to the earthquake. RBS connections are utilized to obtain strong column-weak beam behavior, especially when the beam has a higher moment capacity than the column.

The straight cut was the first recommended form of RBS. Afterward, a linear decreasing cross-section reduction pattern (tapered cut) was introduced. This geometry was proposed due to the increased moment towards the column face. Experimental works showed that both reduced cross-section models performed at high ductility rates. However, cracks and fractures were observed at points where the sudden cross-sectional change occurred. This was because cracks occurred in small notches that are invisible to the naked eye due to the cuts made on the flanges. Studies continued to eliminate this drawback, and it was observed that small notches that occur in suddenly changing sections did not occur in circular cut cross-sections. Thus, the final shape of the reduced beam section proposed by the design codes was accepted as a radius-cut reduced beam section. The radius-cut shape ensures the uniform spread of the plastic hinge in the reduced cross-section (Tezer, 2005).

The possible plastic hinge zones in special moment frames (SMF) are referred to as "protected zones." The protected zone for RBS moment connections extends from the column face to the end of the reduced beam section (Figure 1). Drilling, sudden cross-sectional changes, the use of shear studs, and welding (heat treatment) are not allowed in the protected zone since they could have a negative effect on non-linear behavior.
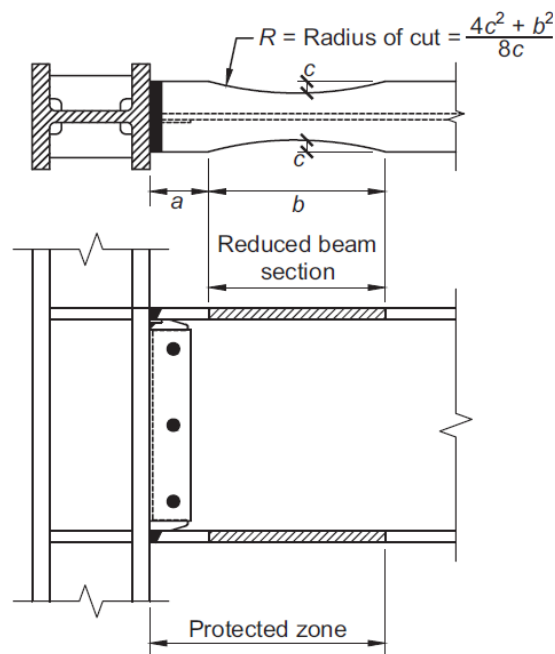

Figure 1. RBS connection. (ANSI/AISC 358-16, 2016).

Prequalification limits are recommended for RBS moment connections in AISC 358-16 as shown in Table 1. If these limits are exceeded, the sufficiency of connection performance should be demonstrated by experimental or analytical studies.

Table 1. AISC/ANSI 358-16 prequalification limits, Source: (ANSI/AISC 358-16, 2016).

Connection details	Prequalification limits
Beam depth shall be limited to a maximum	≤ 920 mm
Beam weight shall be limited to a maximum	≤ 447 kg / m
The clear span-to-depth ratio of the beam shall be limited for SMF systems	≥ 7
The clear span-to-depth ratio of the beam shall be limited for IMF systems	≥ 5
Beam flange thickness shall be limited to a maximum	≤ 44 mm
Beam depth shall be limited to a maximum	≤ 920 mm

There are many studies conducted in the past years for RBS moment connections. M Ohsaki et al. (2009) studied the optimum shape of RBS under cyclic loading. ABAQUS was used for Finite Element Analysis (FEA). The objective function to be maximized was the plastic dissipated energy. The constraint was given for the maximum equivalent plastic strain at the

welded section at the final state. Studies showed that the energy dissipation capability could be essentially increased by optimization compared with the typical beam with uniform flange width. Swati & Gaurang (2014) performed an experimental study for connections with RBS versus without RBS for Indian profiles. It was observed that specimens without RBS showed insufficient performance due to cracks started at the bottom flange weld whereas the specimen with RBS achieved rotation capacity of 0.02 radians without damage in the welds. C.E. Sofias et al. (2014) studied the behavior of the RBS moment connection subjected to cyclic loading with an extended bolted endplate. Two full-scale experimental studies were conducted using European profiles designed according to Euro Code 8. Output results obtained from experiments were compared with those from numerical simulations.

FEA studies showed good agreement with experimental studies. In both specimens, connection elements (endplate, column flange, bolts, welds) remained in the elastic limits due to plastic deformation in the RBS zone. Keunyeong Oh et al. (2015) studied the seismic behavior of weak axis column-tree connections used in steel moment-resisting frames. Specimens with the reduced and tapered beam section showed ductile behavior and successfully reached a 5% story drift ratio without brittle fracture. Although specimen without RBS reached a 5% story drift ratio, brittle fracture was observed at the backing bars. Experimental studies showed that the RBS concept may be the best solution alternative to weak-axis column-tree connections. R. Rahnavard et al. (2015) studied RBS connections with different shape of reducing beam flange and compared with each other during cyclic behavior. ABACUS software was used for FEA analysis. Studies showed that the RBS model using varied holes showed better performance than other models in terms of energy dissipation and also has a minimum magnitude of out of plane buckling. A. Crisan and D. Dubina (2016) examined the plastic mechanism of short steel beams with RBS applied in moment-resisting frames. An alternative method allowing the use of beam FEA for bending–shear interactions was proposed. This method also provided advantages for the analysis of multi-story structures.

M. A. Morshedi et al. (2017) studied the seismic performance of a double reduced beam section (DRBS) using FEA. DRBS is composed of two adjacent radius cut in beam flanges. A parametric study was performed to observe the cut parameters' influence on the seismic performance of the connection. The results showed that DRBS connections have superior hysteretic performance characteristics over RBS connections. R. Li et al. (2017) reported cyclic test results of four composite joints with reduced beam sections. Studies showed that composite joints with RBS performed well under cyclic loading. Some design recommendations and standards, such as FEMA-350 and Eurocode-8 part 3, were mostly based on research on joints without floor slabs. In fact, steel beams were often connected by reinforced concrete floor slabs. Therefore, it was crucial to examine the performance of the reinforced concrete floor slab and weakened beam cross-section connection together. In the study, the experimental study of weakened beam cross-section steel frames with the reinforced concrete floor slab was performed and it was found that these joints exhibit sufficient performance under cyclic load similar to joints without floor slab.

This study investigates the effect of RBS geometry on joint behavior (elastic and plastic stiffness, elastic moment capacity, elastic rotation angle) and seismic performance using ANSYS finite element analysis software. European profiles are preferred in the simulations due to the limited number of studies conducted with European profiles and steel quality in the literature. First, the finite element model is verified using an experimental study in the literature, and then FEA studies are carried out under two different loading types. Under monotonic loading, the effect of the joint geometry on the support behavior characteristic is examined. Besides, regression analysis is conducted utilizing the findings of the FEA under monotonic load, and formulas are developed to provide the elastic-plastic stiffness, elastic moment capacity, and elastic rotation angle of RBS joints for various geometries. Under cyclic loading, the effect of the RBS connection shape on the seismic performance and behavior of the joint is examined. The question of whether RBS joints produced using European steel profiles meet the minimum performance criteria outlined in the earthquake code (AISC/ANSI 341-16, 2016) is also thoroughly investigated.

2. Verification study

FEA is verified based on the experimental study performed by D.T. Pachoumis et al. (2010). In this study, two experiments are performed by using the HE300B profile as a column and the HE180A profile as a beam. The column height is 1797 mm and The beam length is 1200 mm. The loading is applied at a distance of 1000 mm from the face of the column, and moment values are measured from the column face. 10 mm thick continuity plate and 12 mm thick

web doubler plates are used in the panel zone of the connections. The column-beam connection is considered as a fully penetrated groove weld. Finite element verification is performed on RBS$_a$ sample. The dimensions of the reference work are presented in Table 2 and Figure 2.

Table 2. Dimensions of the verification study. Source: (Pachoumis et al., 2010).

Specimens	b$_b$ (mm)	h$_b$ (mm)	a (mm)	b (mm)	c (mm)	s (mm)	r (mm)
RBS$_a$	180	171	144	128.25	36	208.125	75.11

    In this study, a numerical model is developed in the ANSYS (2018) program to examine the performance of the RBS connection under both monotonic and cyclic loads. An experimental study from previous studies is used for verification of the numerical model. Non-linear behavior of the material and the geometry are considered in the Finite Element Analysis (FEA).
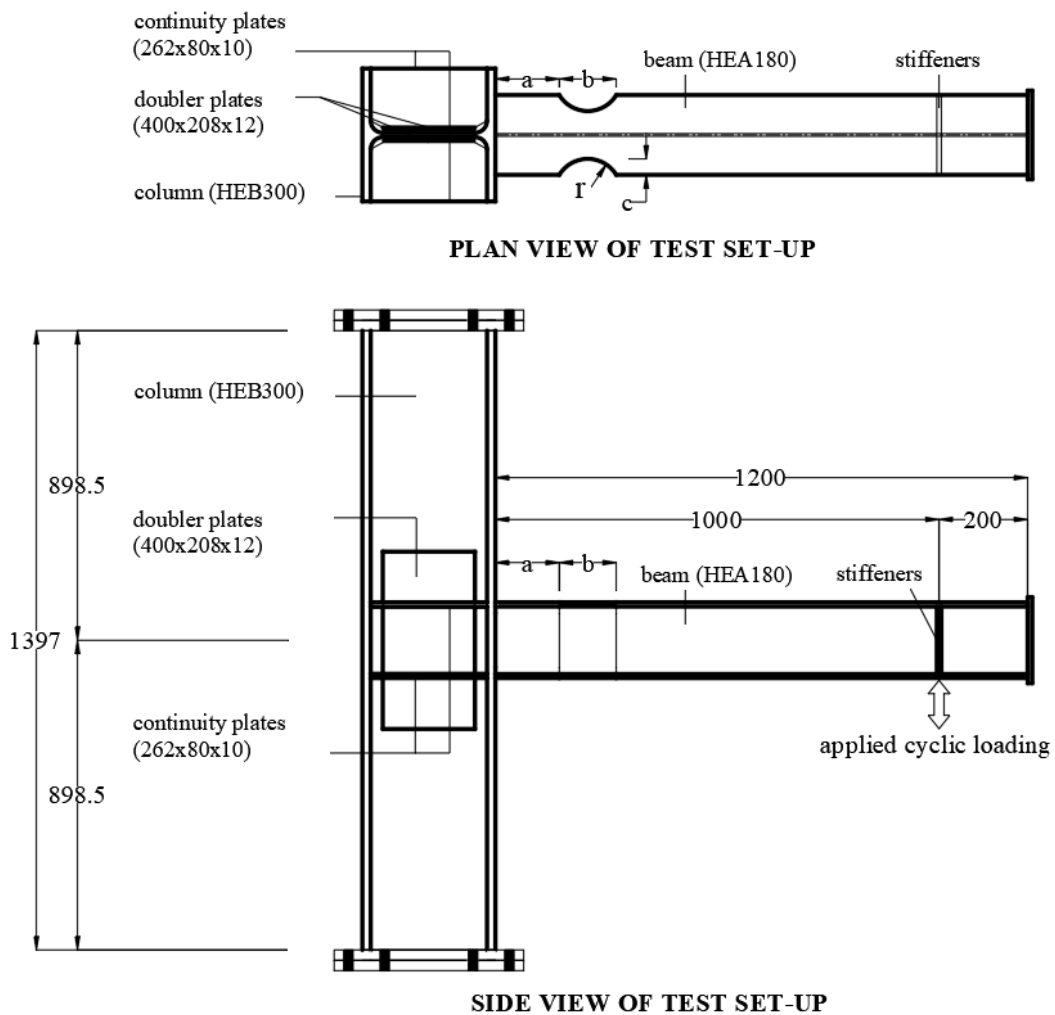

Figure 2. Test setup and connection detail.

2.1. *Finite element model*

All solid elements are modeled using the SOLID186 element, a 3-D 20-node solid element supporting plasticity and large strain capabilities. SOLID186 is generally preferred in steel and similar materials. Contact elements are used on the contact surfaces. Contact elements between solid parts are modeled using TARGE170 and CONTA174. CONTA174 is an 8-node element designed for rigid-flexible and flexible-flexible contact analysis. It can be applied to simulate the contact situation between solid bodies or shells. The TARGE170 element is used to represent the target surfaces for the contact (CONTA174) elements (ANSYS, 2018).

2.2. *Material model*

Steel hardening is commonly explained by two different approaches. These approaches are isotropic and kinematic hardening models. In isotropic hardening, the yield surface expands in all directions, while in kinematic hardening, the yield surface remains constant and shifts in the flow direction. The isotropic hardening model gives very good results under monotonic loading. However, the isotropic material model is insufficient under cyclic loading and cannot adequately simulate the Bauschinger effect. Real steel exhibits some isotropic and some kinematic hardening behavior (Ermeydan, 2019).

In monotonic loading, a bilinear isotropic hardening material model is used for the column, beam, continuity plate, and web doubler plate. According to the study (Pachoumis et al.,2010), the yield strength, tensile strength, and modulus of elasticity of the beam are 310 MPa, 430 MPa, and 209000 MPa. Since all elements except the beam remain elastic during loading, the beam material values are also defined for the other elements. The Poisson ratio is taken as 0.3 for all steel parts. The tangent modulus is assumed to be 6000 MPa (1/35 of the elasticity modulus). The Von Mises yield criterion is employed to investigate the yield of material.

In cyclic loading, a combined (isotropic + kinematic) hardening material model is used for the column, beam, continuity plate, and doubler plate. The Poisson ratio of the material is defined as 0.3. Material yield strength is taken as 310 MPa. The tangent modulus is chosen as 6000 MPa (1/35 of the elasticity modulus).

2.3. *Boundary conditions and load application*

Considering the experimental work used in the verification study, the column ends were defined as fixed supports. The displacement load was applied to the system at the beam tip. In monotonic loading, the displacement load is applied within 10 seconds and in 0.1 second steps with a displacement of 100 mm to the beam end. Beam displacement readings are taken at 1000 mm from the face of the column. In cyclical loading, similar to the reference study (Pachoumis et al., 2010), the loading protocol in the AISC 341-02 earthquake code is implemented as shown in Table3 and Figure 3.

In the verification study, the rotation was determined at the RBS center, while in the parametric study, the total joint rotation was considered by using the beam tip displacement. Besides, moment values were measured at the column center rather than the column face to consider the column's contribution to connection behavior.

Table 3. AISC seismic provisions 341-02 loading protocol used by D.T. Pachoumis and others (2010).

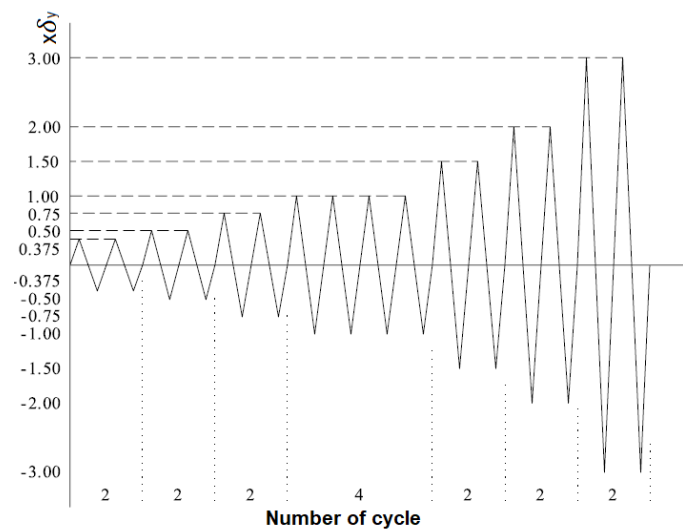| Loading step	Maximum elastic displacement, δ_y	Number of cycle, n
1	0.375	2
2	0.500	2
3	0.750	2
4	1.000	4
5	1,500	2
6	2.000	2
7	3.000	2
8	4.000	2
9	5.000	2
10	6.000	2
11	7.000	2
12	8.000	2
13	9.000	2
14	10.00	2

Figure 3. AISC seismic provisions loading protocol used by D.T. Pachoumis and others (2010).

2.4. *Generation of the moment-rotation curve*

The finite element validation study is implemented in the same way as experimental work using rotation values obtained at the center of the RBS according to Equation 1. Moreover, the moment values are obtained at the column face. Figure 4 shows the location of transducers used in experimental work.

$$\varphi_{RBS} = a\,tan(\frac{\delta_{dtx6} - \delta_{dtx7}}{d_2}) \tag{1}$$

After verifying the finite element study according to equation 1 (Nogueiro, Simões Da Silva, Bento, & Simões, 2006), the rotation values of the parametric studies are read from the beam tip and obtained utilizing equation 2 (Nogueiro et al., 2006)

$$\varphi_{total} = a\,tan(\frac{\delta_{dty1}}{L_1}) \tag{2}$$

Equation 3 (Nogueiro et al., 2006) is used to calculate column rotation.

$$\varphi_{column} = a\,tan(\frac{\delta_{dtx10} - \delta_{dtx11}}{d_1}) \qquad (3)$$

Equation 4 (Nogueiro et al., 2006) is used to calculate the rotation of the beam.

$$\varphi_{beam} = \varphi_{total} - \varphi_{column} \qquad (4)$$

φ_{RBS} : Rotation at the center of reduced beam section

φ_{total} : Total rotation

φ_{column} : Column rotation

φ_{beam} : Beam rotation

δ_{dtx} : Displacement in the x direction

δ_{dty} : Displacement in the y direction

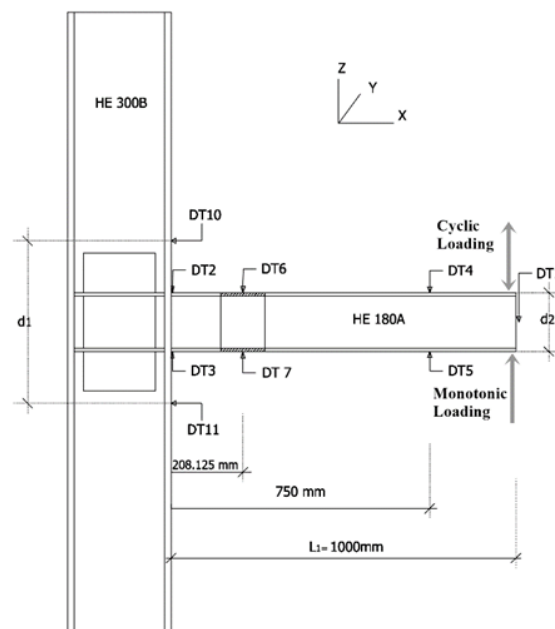d_1 : Distance between displacement points

**Figure 4.** Location of transducers.

2.5. *Evaluation of the verification study results*

The verification study was conducted using the envelope curve obtained from the hysteresis curve. Moment-rotation curves (Figure 5) and failure modes (Figure 6) are obtained from numerical and experimental studies under monotonic and cyclic loading. The connection behavior in the elastic and plastic regions (Figure 5a, b) is sufficiently achieved. Moreover, a good agreement is also observed for the failure modes of numerical and experimental studies, as shown in Figures 6a and 6b. As a result, the finite element model (FEM) successfully simulates the behavior of column-beam connections.
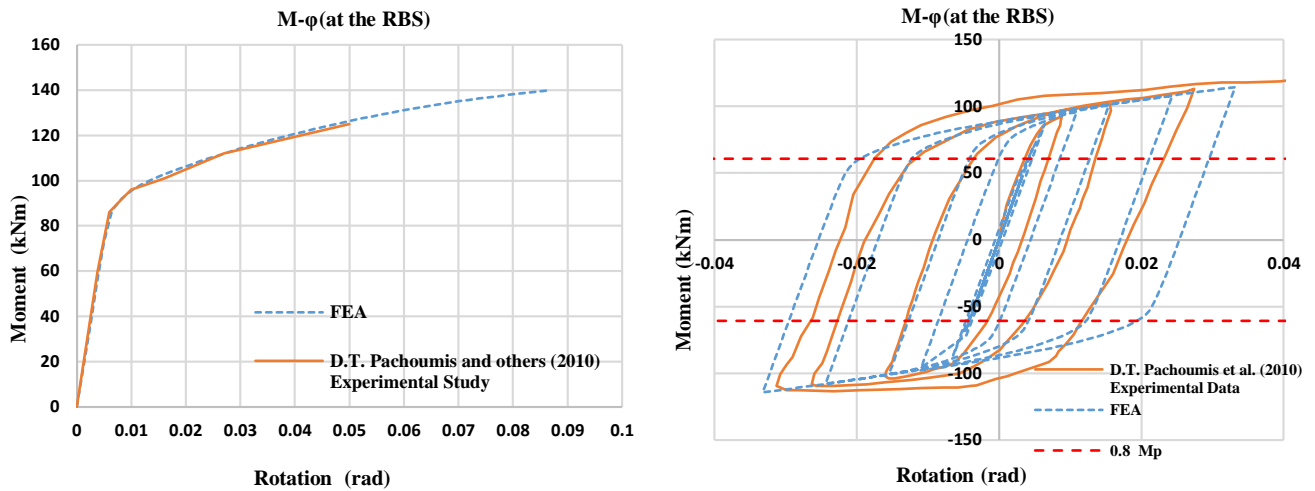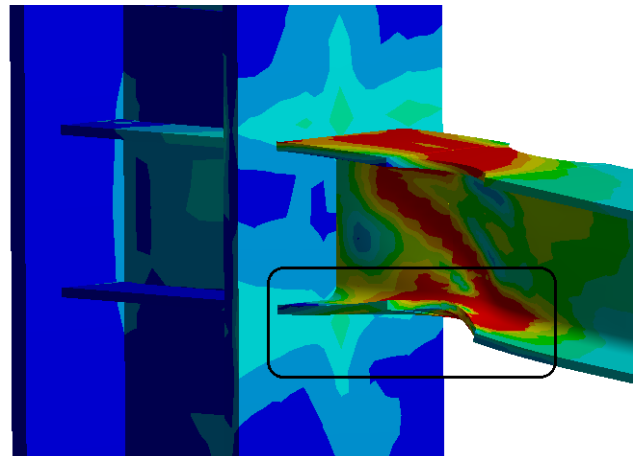
a) Isotropic hardening model under monotonic loading.　　　　b) Combined hardening model under cyclic loading.
Figure 5. Verification of FEA under monotonic and cyclic loading.
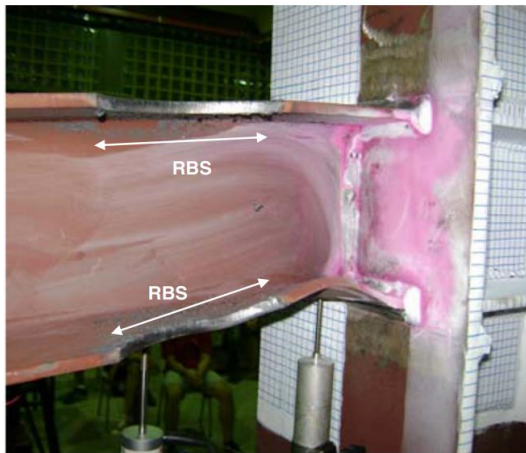
a) Bottom flange buckling of specimen at 0.11 radian (EXPERIMENT). Source: (Pachoumis et al., 2010)　　b) Bottom flange buckling of specimen at 0.11 radian (FEA). Source: (Self-Elaboration)

Figure 6. Failure mode obtained from FEA and experiment.

3. Parametric study

3.1. *Parametric study under monotonic loading*

A parametric study is conducted after the verification study is successfully completed. Beam size, beam length, column size, column length, the distance between the beginning of RBS to the column flange (a), length of RBS (b), depth of cross-section reduction (c), and connection types without RBS are determined as key parameters to evaluate the seismic performance of RBS connections (Figure 2). These parameters are compared with each other, and their effects on connection behavior are investigated. Moment-total rotation (inter-story drift angle) plots of the connections are generated under monotonic loading for the selected parameters. As a result of the FEA parametric study performed under monotonic loading, the following points are observed.

3.1.1. Effect of "a" length on connection behavior

The column-beam connection's stiffness and plastic moment capacity slightly increase with the increase of the length "a" between the beginning of the reduced beam cross-section and the column face. As the length of "a" increases from 90 mm to 120 mm, the stiffness increases 0.25% in the elastic region and 1.7% in the plastic region. On the other hand, by increasing the length "a" from 90 mm to 120 mm, the plastic moment capacity increases by 2.5% (Figure 7a).

3.1.2. Effect of "b" length on connection behavior

Column-beam connection stiffness and plastic moment capacity slightly decrease with the increase in length "b" of the weakened beam cross-section. As the "b" increases from 115 mm to 145 mm, the rigidity decreases by 0.4% in the elastic region and 0.5% in the plastic region. On the other hand, with the increase of "b" from 115 mm to 145 mm, the plastic moment capacity decreases by 0.4%. The variation of the length "b" is not considered when obtaining the equation, as it hardly affects the capacity of the connection (Figure 7b).

3.1.3. Effect of "c" length on connection behavior

The column-beam connection's stiffness and the plastic moment capacity significantly decrease as the cross-section reduction depth "c" increases in the beam flange. As the "c" increases from 20 mm to 40 mm, the stiffness decreases by 5% in the elastic region and 10.2% in the plastic region. On the other hand, with the increase of "c" from 20 mm to 40 mm, the plastic moment capacity decreases by 11.7% (Figure 7c).

3.1.4. Effect of beam size on connection behavior

As the beam size increase, connection stiffness and plastic moment capacity increase. When the HE 300A profile is used instead of the HE 180A profile, the stiffness increases by 240% in the elastic region and 202% in the plastic region. Plastic moment capacity increases by 210% (Figure 7d).

3.1.5. Effect of beam length on connection behavior
It is observed that column-beam connection stiffness and plastic moment capacity decrease with increasing beam length. As the beam length increases from 1000 mm to 3000 mm, the stiffness decreases by 55.8% in the elastic zone and 23.9% in the plastic zone. On the other hand, with the increase in the beam length from 1000 mm to 3000 mm, the plastic moment capacity decreases by 29.8%. (Figure 7e).

3.1.6. Effect of column size on connection behavior

It is observed that the column-beam connection stiffness and plastic moment capacity increase significantly as the column profile increases in size. As the column profile increases from HE 200B to HE 600B, the stiffness increases by 128.6% in the elastic zone and 65% in the plastic zone. On the other hand, as the column profile increases from HE 200B to HE 600B, the plastic moment capacity increases by 49.7% (Figure 7f).

3.1.7. Effect of column length on connection behavior

It is seen that the column-beam connection stiffness and plastic moment capacity increase slightly with increasing column length. As the column length increases from 1797 mm to 5000 mm, the stiffness increases by 3.1% in the elastic region and 2.3% in the plastic region. On the other hand, as the column length increases from 1797 mm to 5000 mm, the plastic moment capacity increases by 1% (Figure 7g).

3.1.8. Effect of change in size of column and beam on connection behavior

Column and beam profiles are examined by changing their sizes together, considering the principle of strong column-weak beam. It is observed that the column-beam connection stiffness and plastic moment capacity increase as the column and beam profiles increase. The stiffness in the elastic region increases by 1460%, the stiffness in the plastic region increases by 912%, and the plastic moment capacity increases by 852% as we moved from the HE 200B column-HE 140A beam profile connection to the HE 600B column-HE 300A beam connection (Figure 7h).

3.1.9. Comparison of RBS and without RBS connections

Figure 7j illustrates the stiffness change in elastic and plastic regions for the models with and without RBS. The elastic and plastic stiffness of the model without RBS are 8.7% and 17% higher than those of the model with RBS, respectively. In addition, the plastic moment capacity of the model without RBS is 21.9% higher than the plastic moment capacity of the model with RBS.

Table 4. Monotonic test results.

Models	b_f (mm)	d_b (mm)	a (mm)	b (mm)	c (mm)	Column Profile	Beam Profile	Column Height(mm)	Beam length (mm)	%0.5 Rotation moment (kNm)	%4 Rotation moment (kNm)	M_p (kNm)
Verified	180	171	*144*	128.25	36	HEB 300	HEA 180	1797	1000	48.597	130.110	115.691
A1	180	171	*90*	128.25	36	HEB 300	HEA 180	1797	1000	48.228	125.930	110.717
A2	180	171	*100*	128.25	36	HEB 300	HEA 180	1797	1000	48.224	126.570	111.595
A3	180	171	*110*	128.25	36	HEB 300	HEA 180	1797	1000	48.321	127.290	112.498
A4	180	171	*120*	128.25	36	HEB 300	HEA 180	1797	1000	48.349	128.080	113.465
Verified	180	171	144	*128.25*	36	HEB 300	HEA 180	1797	1000	48.597	130.110	115.691
B1	180	171	144	*115*	36	HEB 300	HEA 180	1797	1000	48.672	130.38	115.881
B2	180	171	144	*125*	36	HEB 300	HEA 180	1797	1000	48.616	130.17	115.745
B3	180	171	144	*135*	36	HEB 300	HEA 180	1797	1000	48.557	129.98	115.583
B4	180	171	144	*145*	36	HEB 300	HEA 180	1797	1000	48.483	129.8	115.433
Verified	180	171	144	128.25	*36*	HEB 300	HEA 180	1797	1000	48.597	130.110	115.691
C1	180	171	144	128.25	*20*	HEB 300	HEA 180	1797	1000	50.443	141.100	127.141
C2	180	171	144	128.25	*25*	HEB 300	HEA 180	1797	1000	49.924	138.050	124.038
C3	180	171	144	128.25	*30*	HEB 300	HEA 180	1797	1000	49.331	134.630	120.614
C4	180	171	144	128.25	*40*	HEB 300	HEA 180	1797	1000	47.907	126.740	112.247
Verified	180	171	144	128.25	36	HEB 300	*HEA 180*	1797	1000	48.597	130.110	115.691
D1	140	133	90	100.00	25	HEB 300	*HEA 140*	1797	1000	25.595	69.470	61.023
D2	220	210	135	155.00	40	HEB 300	*HEA 220*	1797	1000	79.236	209.090	188.155
D3	260	250	165	185.00	45	HEB 300	*HEA 260*	1797	1000	121.671	302.670	278.709
D4	300	290	185	215.00	55	HEB 300	*HEA 300*	1797	1000	165.164	393.010	359.544
Verified	180	171	144	128.25	36	HEB 300	HEA 180	1797	*1000*	48.597	130.110	115.691
E1	180	171	144	128.25	36	HEB 300	HEA 180	1797	*1500*	36.739	116.240	101.298
E2	180	171	144	128.25	36	HEB 300	HEA 180	1797	*2000*	29.612	108.270	92.802
E3	180	171	144	128.25	36	HEB 300	HEA 180	1797	*2500*	24.936	103.740	86.732
E4	180	171	144	128.25	36	HEB 300	HEA 180	1797	*3000*	21.494	102.120	81.259
Verified	180	171	144	128.25	36	*HEB 300*	HEA 180	1797	1000	48.597	130.110	115.691
F1	180	171	144	128.25	36	*HEB 200*	HEA 180	1797	1000	32.914	87.966	96.192
F2	180	171	144	128.25	36	*HEB 400*	HEA 180	1797	1000	59.183	139.590	121.523
F3	180	171	144	128.25	36	*HEB 500*	HEA 180	1797	1000	67.450	145.980	126.447
F4	180	171	144	128.25	36	*HEB 600*	HEA 180	1797	1000	75.257	152.280	131.693
Verified	180	171	144	128.25	36	HEB 300	HEA 180	*1797*	1000	48.597	130.110	115.691
G1	180	171	144	128.25	36	HEB 300	HEA 180	*2500*	1000	48.629	131.010	115.976
G2	180	171	144	128.25	36	HEB 300	HEA 180	*3000*	1000	48.013	130.750	115.497
G3	180	171	144	128.25	36	HEB 300	HEA 180	*4000*	1000	48.801	132.060	116.876
G4	180	171	144	128.25	36	HEB 300	HEA 180	*5000*	1000	50.112	133.110	116.805

|												
Verified	180	171	144	128.25	36	*HEB 300*	*HEA 180*	1797	1000	48.597	130.110	115.691
H1	140	133	90	100.00	25	*HEB 200*	*HEA 140*	1797	1000	18.849	60.108	56.009
H2	200	190	125	140.00	35	*HEB 400*	*HEA 220*	1797	1000	78.560	190.150	164.524
H3	240	230	150	170.00	40	*HEB 500*	*HEA 260*	1797	1000	150.388	347.590	308.904
H4	300	290	185	215.00	55	*HEB 600*	*HEA 300*	1797	1000	293.931	608.650	533.491
Verified	180	171	*144*	*128.25*	*36*	HEB 300	HEA 180	1797	1000	48.597	130.110	115.691
Without RBS	180	171	*0*	*0.00*	*0*	HEB 300	HEA 180	1797	1000	64.569	158.370	140.965
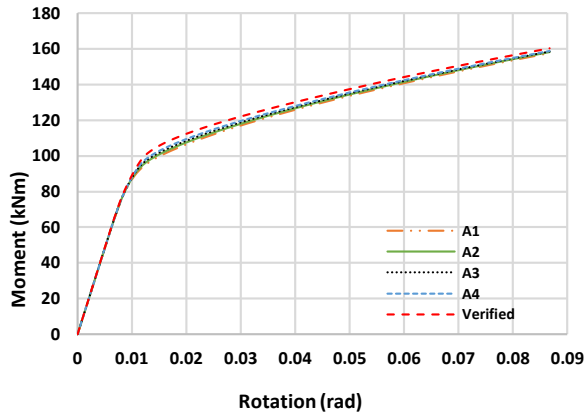
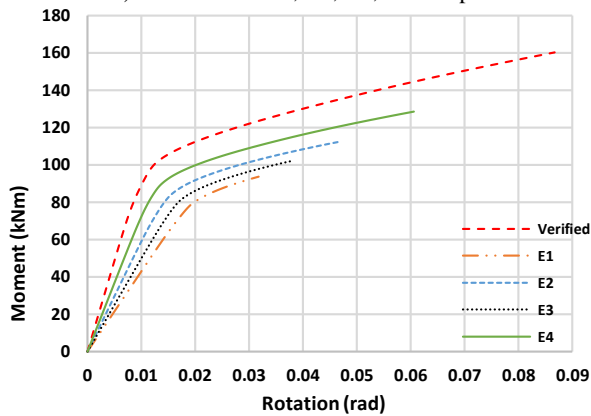a) Verified and A1, A2, A3, A4 comparison.
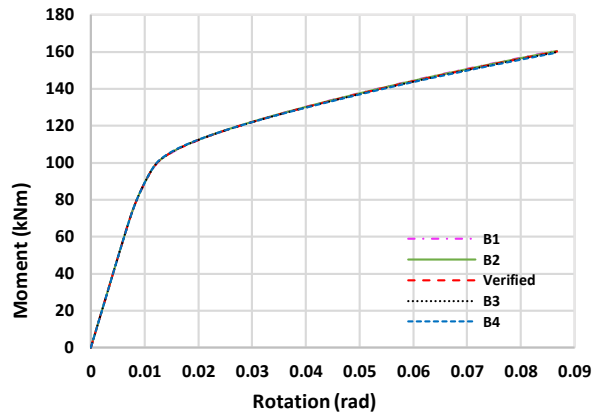
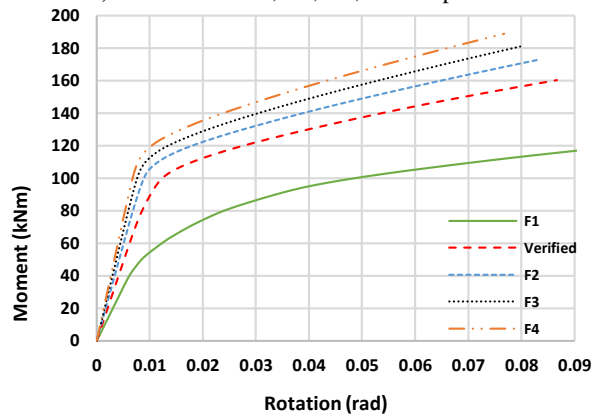
b) Verified and B1, B2, B3, B4 comparison.
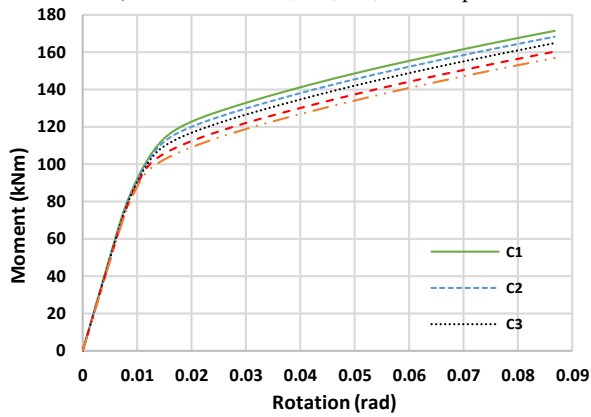
c) Verified and C1, C2, C3, C4 comparison.
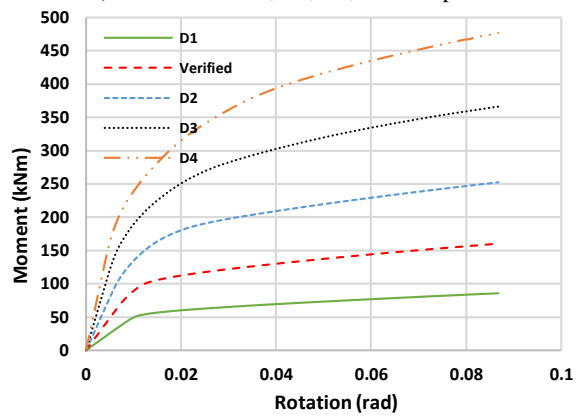
d) Verified and D1, D2, D3, D4 comparison.

e) Verified and E1, E2, E3, E4 comparison.
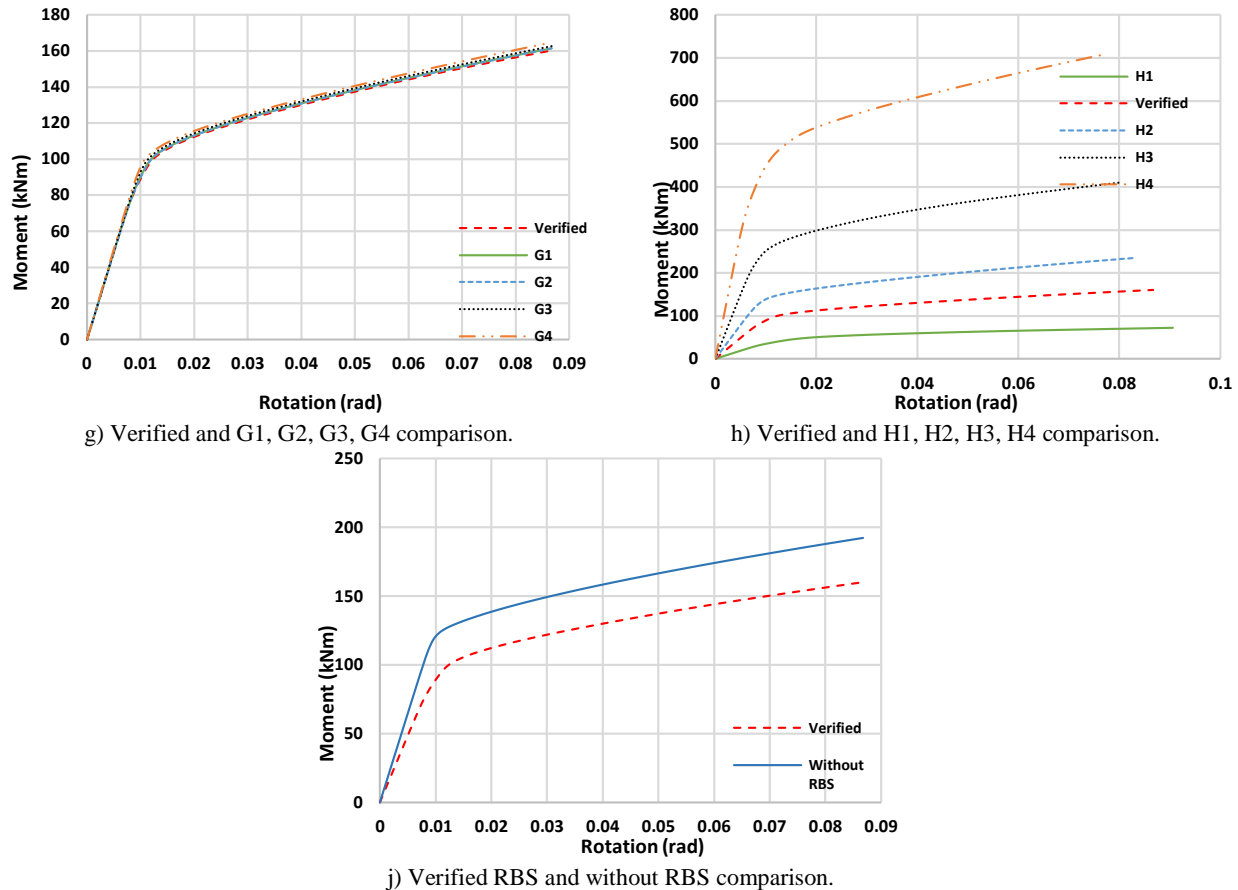

f) Verified and F1, F2, F3, F4 comparison.

g) Verified and G1, G2, G3, G4 comparison.

h) Verified and H1, H2, H3, H4 comparison.

j) Verified RBS and without RBS comparison.

Figure 7. Moment-rotation curves under monotonic load.

3.2. *Parametric study under cyclic loading*

In the second part of the parametric study, RBS models with various dimensions (a, b, and c) and the model without RBS are examined under cyclic loading (Figure 8) using the ANSYS (2018) FEA program. Figure 8a presents the contribution of the column to the total rotation. The column exhibits elastic behavior throughout the simulation. Figure 8b displays the contribution of the beam to the total rotation and plasticization occurs entirely within the beam. The horizontal dashed line in the Figures 8c, 8d, 8e, and 8f. represents 20% of the beam moment capacity. These models have a strength greater than 80% of the beam moment capacity at 0.04 radians of rotation. The following observations are made at the conclusion of the cyclic loading analysis.

3.2.1. Comparison of RBS and without RBS connections

Figure 8c illustrates the stiffness change in elastic regions for the models with and without RBS. The elastic stiffness of the model without RBS is 12.3% higher than the model with verified RBS. In addition, the plastic moment capacity of the model without RBS is 31.7% higher than the plastic moment capacity of the model with verified RBS. The moment capacity of the model without RBS at 4% rotation is determined to be 17.8% higher than the moment capacity of the model with verified RBS (Table 5).

3.2.2. Effect of "a" length on connection behavior

Figure 8d displays the stiffness changes in elastic regions for the verified RBS and the A1 model. a = 144 mm in the verified model and a = 90 mm in the A1 model. The elastic stiffness of the verified RBS model is 15.6% higher than the A1 model. In addition, the plastic moment capacity of the verified RBS model is 24.8% higher than the plastic moment capacity of the A1 model. The moment capacity of the verified RBS model at 4% rotation is 17.8% higher than the moment capacity of the A1 model (Table 5).

3.2.3. Effect of "b" length on connection behavior

Figure 8e shows the stiffness changes in elastic regions for the verified RBS and B4 models. b= 128.25 mm in the verified model and b = 145 mm in the B4 model. The elastic stiffness of the verified RBS model is 0.4% higher than the B4 model. In addition, the plastic moment capacity of the verified RBS model is 0.8% higher than the plastic moment capacity of the B4 model. The moment capacity of the verified RBS model at 4% rotation is determined to be 0.5% higher than the moment capacity of the B4 model (Table 5).

3.2.4. Effect of "c" length on connection behavior

Figure 8f illustrates the stiffness change in elastic regions for the verified RBS and C1 models. c= 36 mm in the verified RBS model and c = 20 mm in the C1 model. The elastic stiffness of the C1 model is 4.9% higher than the model verified RBS. In addition, the plastic moment capacity of the C1 model is 9.7% higher than the plastic moment capacity of the model verified RBS. The moment capacity of the C1 model at 4% rotation is determined to be 9.1% higher than the moment capacity of the verified RBS model (Table 5).

Table 5. Cyclic test results.

| Model	Verified RBS	Without RBS	A1	B4	C1
Column profil	HE300B	HE300B	HE300B	HE300B	HE300B
Beam profil	HE180A	HE180A	HE180A	HE180A	HE180A
b_f (mm)	180.000	180	180.000	180.000	180.000
d_b (mm)	171.000	171	171.000	171.000	171.000
a (mm)	144.000	0	90.000	144.000	144.000
b (mm)	128.250	0	128.250	145.000	128.250
c (mm)	36.000	0	36.000	36.000	20.000
s (mm)	208.125	-	154.125	216.500	208.125
R (mm)	75.110	0	75.110	91.000	112.800
0.8Mp(kNm)	60.899	92.271	60.899	60.899	74.842
%4 Rotation moment (kNm)	135.490	176.420	114.970	134.880	147.840
M_p (kNm)	109.744	144.495	87.951	108.836	120.431
Elastic stiffness	12148.600	13641.300	10510.900	12097.400	12743.300
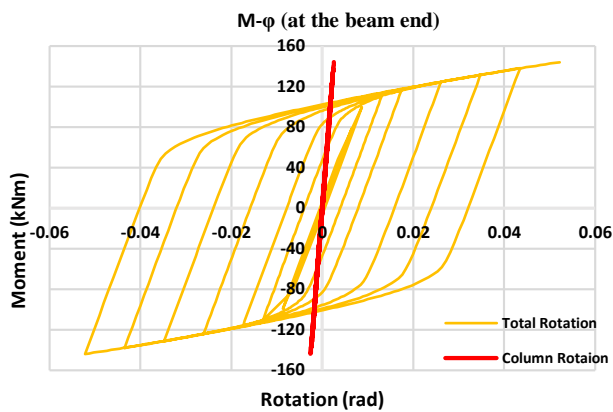
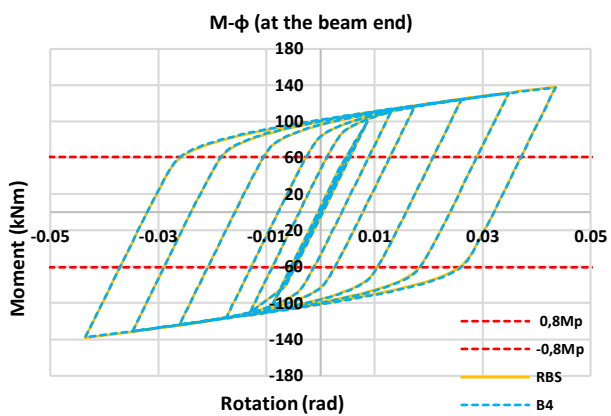a) The contribution of column to total rotation.
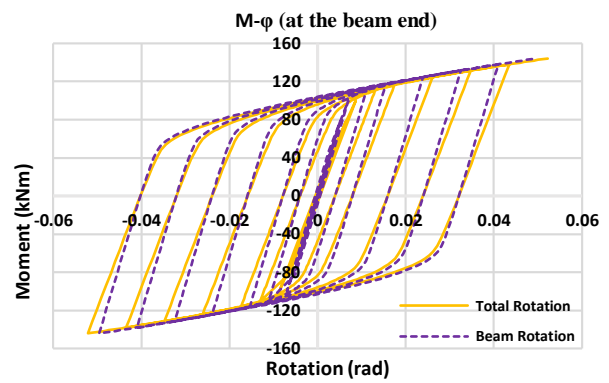
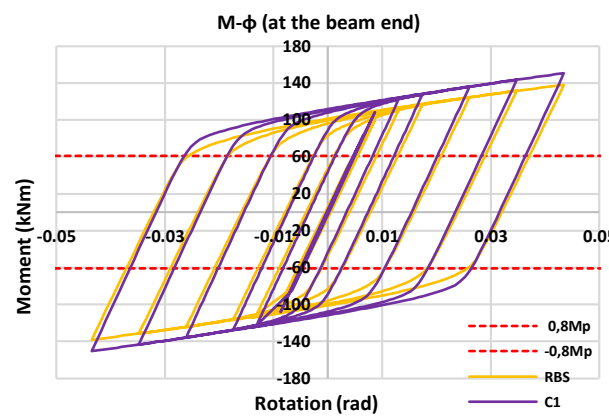b) The contribution of beam to total rotation.
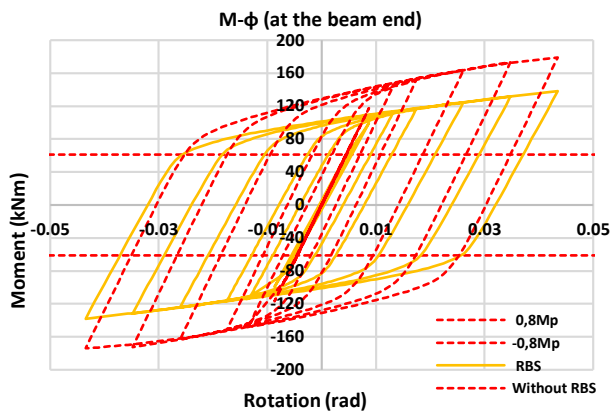
c) Verified RBS and Without RBS comparison
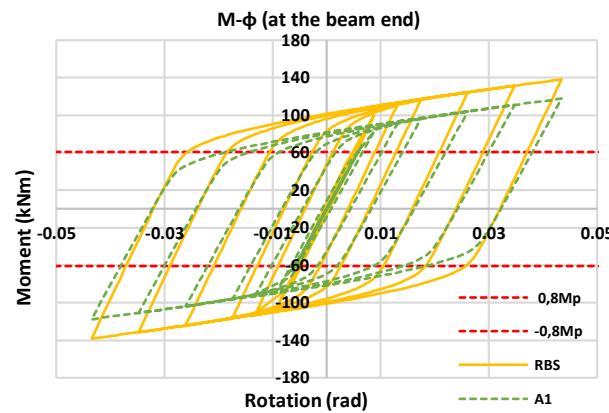
d) Verified and A1 comparison

e) Verified and B4 comparison

f) Verified and C1 comparison

Figure 8. Moment-rotation curves under cyclic load.

3.3. *Plastic hinge location*

In SMF frames, it is aimed to form earthquake energy dissipation zones (plastic hinges) at the beam end. The connection and column are designed to be stronger than the beam utilizing the moments at the column's center and on its face. Plastic hinge's location must be specified to compute these moments. Equations 5 and 6 (ANSI/AISC 358-16, 2016) below show the calculation of the moment occurring in the center of the column and on the face of the column.

$$M_f = M_{pr} + V_p x \qquad (5)$$

$$M_c = M_{pr} + V_p \left(x + \frac{d_c}{2} \right) \qquad (6)$$

Where M_{pr} is the plastic connection bending capacity, V_p is the plastic connection shear force, x is the distance of the plastic connection from the column face, M_f is the moment occurring on the column face, and M_c is the moment occurring at the center axis of the column. In this study, the location of the plastic hinge is investigated (Figure 9a-9e) under cyclic loading using PEEQ index values depending on changing RBS geometries. The PEEQ index given in Equation 7 (Chen, Chen, Chung, & Lin, 2005) is the ratio of equivalent plastic strain to yield strain. ε_{ij} denotes the plastic strain component in the directions indicated by i and j. The increase of the PEEQ index for a certain region is evaluated as the increase in the crack, damage, or deformation potential that may occur in that region.

$$PEEQ \ index = \left(\sqrt{\frac{2}{3} \varepsilon_{ij} \varepsilon_{ij}} \right) / \varepsilon_y \qquad (7)$$

PEEQ index changes are examined in the beam web (Figure 9a-9e). The change of plastic hinge location depending on the RBS geometry is given below.

- As the length of "a" increases, the location of the plastic hinge moves away from the column face. The plastic hinge is formed at 166.67 mm from the column in the model with a = 144 mm, while it is formed at 116.67 mm in the A1 model with a = 90 mm (Figures 9a and 9c).
- It is observed that the plastic hinge location is not affected due to the change in length "b". The plastic hinge occurred at 166.67 mm from the column face in the verified model with b = 128.25 mm and the B4 model with b = 145 mm (Figures 9a and 9d).
- In the model without RBS, the plastic hinge occurs in a region closer to the column face compared to the RBS model. The plastic hinge occurred at 166.67 mm in the verified RBS model and 66.67 mm in the model without RBS from the column face. The figures (Figures 9a and 9b) show that the use of RBS successfully moves away plasticization from the column and connection zone.
- As the depth of "c" decreases, the location of the plastic hinge occurs closer to the column face. The plastic hinge is formed at 166.67 mm from the column in the model with c = 36 mm, while it is formed at 150 mm in the C1 model with c = 20 mm (Figures 9a and 9e).
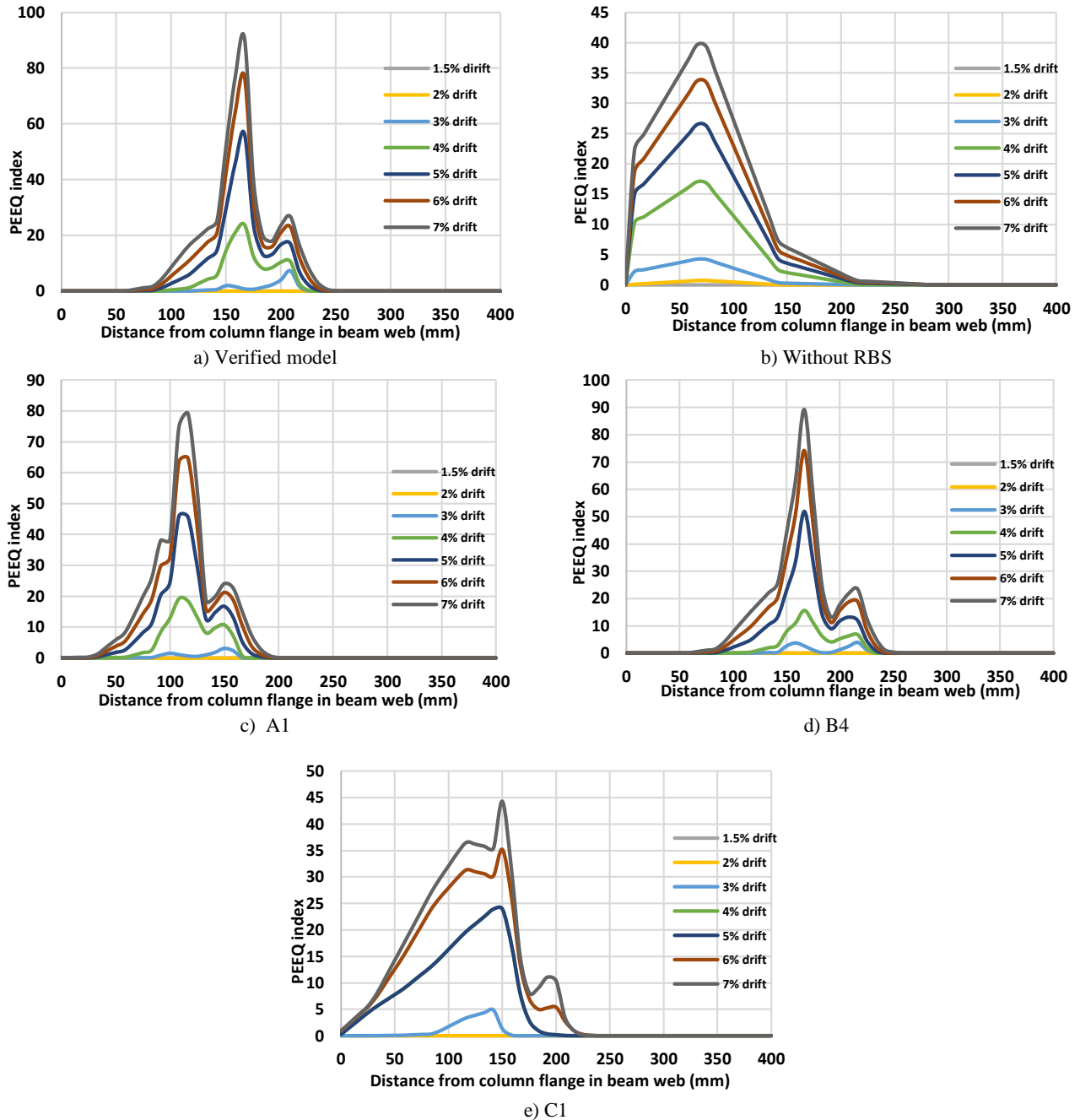
Figure 9. PEEQ index values along the beam length at different story drifts.

4. Correlation study

In this section, a multi-linear regression analysis is performed. For this purpose, the results obtained from 30 finite element analyses under monotonic loading are imported into the DATAFIT (2014) program. The distance between the column face and the beginning of RBS (a), RBS weakening depth (c), plastic section modulus of the beam (W_{plyb}), beam length (L_b), plastic section modulus of column (W_{plyc}), and column length (L_c) are selected as parameters. As a result, four empirical formulas that give elastic moment capacity (M_p), elastic rotation capacity (φ_p), elastic ($K_{elastic}$), and plastic ($K_{plastic}$) stiffness of RBS connections are generated.

$$\varphi_p = 0.695a - 2.328c + 0.201\,L_b - 10.993\,W_{plyb} - 0.003L_c - 71.076W_{plyc} - 4.505 \tag{8}$$

$$M_p = 94.449a - 958.052c - 14.578\,L_b + 147652.38\,W_{plyb} + 3.194L_c + 13428.312W_{plyc} + 65.737 \tag{9}$$

$$K_{elastik} = -2627.12a - 65176.15c - 2274.96\,L_b + 13912983.11\,W_{plyb} + 340.10L_c + 1738482.58W_{plyc} + 5671.30 \tag{10}$$

$$K_{plastik} = -314.668a - 4.047c + 200.124L_b + 540500.774W_{plyb} + 25.254L_c + 78170.501W_{plyc} + 44.512 \tag{11}$$

Table 6. Statistical coefficients between ANSYS results and equation results.

Equation	r	NSCE	MRE	CRMSE %
M_p	0.979	0.96	-9.18×10^{-11}	14
φ_p	0.920	0.85	-0.23×10^{-3}	7
$K_{elastik}$	0.981	0.96	-1.59×10^{-15}	13
$K_{plastik}$	0.974	0.95	7.81×10^{-16}	12

4.1. Obtaining statistical coefficients

4.1.1. Correlation coefficient (r)

The value of r varies between -1 and 1. The correlation coefficient describes how well the regression line fits the observed data. As the r-value approaches one, the agreement between the observed data and the simulated data increases. The correlation coefficient for the statistical study is calculated according to Equation 12 (Dis, Anagnostou, & Mei, 2018).

$$r = \frac{\sum_{i=1}^{n}(X_{r,i} - \overline{X_r})(X_{s,i} - \overline{X_s})}{\sqrt{\sum_{i=1}^{n}(X_{r,i} - \overline{X_r})^2 \sum_{i=1}^{n}(X_{s,i} - \overline{X_s})^2}}, \qquad [-1, 1] \tag{12}$$

Where X_r is the values obtained from ANSYS (2018) numerical analysis program, X_s is the values obtained from the Equation, and $\overline{X}$ is the average of ANSYS (2018) and equation values. The correlation coefficient (r) is r = 1 when there is a perfect positive linear relationship and r = -1 when there is a perfect negative linear relationship. If there is no linear relationship, r = 0.

4.1.2. Nash-sutcliffe efficiency coefficient (NSE)

NSE ranges from $-\infty$ to 1. NSE = 1 indicates that the perfect fit of the generated equation to the observed data. 0<NSE< 1 corresponds to the obtained equation performance within acceptable limits. An NSE value less than 0 indicates that the obtained equation performance is inadequate. The NSE is calculated according to Equation 13 (Dis et al., 2018).

$$NSCE = 1 - \frac{\sum_{i=1}^{n}(X_{r,i} - X_{s,i})^2}{\sum_{i=1}^{n}(X_{r,i} - \overline{X_r})^2}, \qquad [-\infty, 1] \tag{13}$$

4.1.3. Centered Root-Mean-Square Error (CRMSE)

CRMSE ranges from 0 to ∞. As the CRMSE value approaches 0, CRMSE indicates that the generated equation performance is successful. If the CRMSE value is less than 100, it means that the equation performance is acceptable. The CRMSE is calculated according to Equation 14 (Dis et al., 2018).

$$CRMSE = \frac{1}{\overline{X_r}} \sqrt{\frac{\sum_{i=1}^{n}[X_{r,i} - X_{S,i} - (\overline{X_r} - \overline{X_s})]^2}{n}} \times 100\%, \quad [0, \infty] \quad (14)$$

4.1.4. Mean Relative Error (MRE)

The MRE ranges from -∞ to ∞. The success of the equation increases as the MRE value approaches 0. The MRE coefficient is calculated according to Equation 15 (Dis et al., 2018).

$$MRE = \frac{\sum_{i=1}^{n}(X_{s,i} - X_{r,i})}{\sum_{i=1}^{n} X_{r,i}}, \quad [-\infty, \infty] \quad (15)$$

5. Conclusions

In this study, the effect of RBS geometry on column-beam connection behavior and seismic performance are examined under monotonic and cyclic loading using ANSYS (2018) FEA software. Besides, the location of plastic hinges in the RBS connection is investigated in detail, and regression analysis is conducted using simulation studies performed under monotonic load. The main results achieved in the study are presented below.

1. The effect of parameters a, b, and c of RBS geometry on connection behavior is presented in detail in the study. RBS connections are not affected much by the *a* and *b* parameters; however, they are severely affected by the *c* parameter. As the cutting depth (c) increases, strength degradation increases rapidly in the following cycles. In summary, the column-beam connection's moment capacity decreases under monotonic and cyclic loading by using RBS (Figure 7 c-7j and Figure 8c). In this case, it is understood that RBS connections should not be used arbitrarily. The use of RBS seems more effective in the case of a strong beam-weak column behavior occurring in the structural system. The only advantage of using RBS in a connection that provides a strong column-weak beam condition is that the plasticization zone is moved to the desired region away from both the column and the connection of the column and the beam. (Figure 9a-9e). The connection strength must be over 0.8 M_{pb} at 0,04 inter-story drift angle when applying section reduction;
2. Experimental work is successfully simulated in FEA. As a result of the multi-linear regression analysis, using the simulation results under monotonic loading, four equations are derived (Equations 8,9,10, and 11) that will enable us to achieve the moment-rotation behavior of the connection depending on the RBS geometry;
3. Finite element analysis for RBS connections using European steel profiles showed that these profiles meet adequate performance criteria according to AISC/ANSI 341-16 (2016) under cyclic loading;
   Comprehensive studies can be done on the following subjects:
4. The investigated RBS connections in this study are analyzed as welded connections. In future work, the bolted column-beam connections can be examined;
5. In this work, the beam is connected to the strong axis of the column. RBS connections where the beams are connected to the weak-axis of the column should also be studied.

References

ANSI/AISC 341-16. Seismic provisions for structural steel buildings, 11 Construction, American Institute of Steel § (2016). Retrieved from https://www.aisc.org/globalassets/aisc/publications/standards/seismic-provisions-for-structural-steel-buildings-ansi-aisc-341-16.pdf

ANSI/AISC 358-16. Prequalified connections for pecial and intermediate steel moment frames for seismic applications. , American Institute of Steel Construction § (2016). Retrieved from https://www.aisc.org/globalassets/aisc/publications/standards/A358-16W.pdf

ANSYS. (2018). Theory Reference for the Mechanical APDL and Mechanical Applications. After Adoption. Canonsburg, Pennsylvania, U.S.A.: SAS IP, Inc. Retrieved from https://www.ansys.com/academic/students Retrieved from https://www.ansys.com/academic/students

Chen, C.-C., Chen, S.-W., Chung, M.-D., & Lin, M.-C. (2005). Cyclic behaviour of unreinforced and rib-reinforced moment connections. Journal of Constructional Steel Research, 61(1), 1–21. https://doi.org/10.1016/j.jcsr.2004.06.005 Retrieved from https://linkinghub.elsevier.com/retrieve/pii/S0143974X04000951

Crisan, A., & Dubina, D. (2016). Bending–shear interaction in short coupling steel beams with reduced beam section. Journal of Constructional Steel Research, 122, 190–197. https://doi.org/10.1016/j.jcsr.2016.03.020 Retrieved from http://dx.doi.org/10.1016/j.jcsr.2016.03.020

Datafit 9.0. (2014). Datafit. Oakdale,Canada.

Dis, M. O., Anagnostou, E., & Mei, Y. (2018). Using high-resolution satellite precipitation for flood frequency analysis: case study over the Connecticut River Basin. Journal of Flood Risk Management, 11(November 2017), S514–S526. https://doi.org/10.1111/jfr3.12250 Retrieved from http://doi.wiley.com/10.1111/jfr3.12250

Ermeydan, İ. (2019). Investigation performance of steel frames with reduced beam section under cyclic loading. Kahramanmaraş Sütçü İmam University, Graduate School of Natural and Applied Sciences,Kahramanmaraş.

Karip, C. (2014). Comparative performance assessments of steel frames with reduced beam section (rbs) under earthquake loads. İstanbul Technical University, Science Institute, İstanbul.

Li, R., Samali, B., Tao, Z., & Kamrul Hassan, M. (2017). Cyclic behaviour of composite joints with reduced beam sections. Engineering Structures, 136, 329–344. https://doi.org/10.1016/j.engstruct.2017.01.025 Retrieved from http://dx.doi.org/10.1016/j.engstruct.2017.01.025

Morshedi, M. A., Dolatshahi, K. M., & Maleki, S. (2017). Double reduced beam section connection. Journal of Constructional Steel Research, 138, 283–297. https://doi.org/10.1016/j.jcsr.2017.07.013 Retrieved from https://doi.org/10.1016/j.jcsr.2017.07.013

Nogueiro, P., Simões Da Silva, L., Bento, R., & Simões, R. (2006). Experimental behaviour of standardised european end-plate beam-to-column steel joints under arbitrary cyclic loading. Proceedings of the International Colloquium on Stability and Ductility of Steel Structures, SDSS 2006, (February), 951–960.

Oh, K., Lee, K., Chen, L., Hong, S.-B., & Yang, Y. (2015). Seismic performance evaluation of weak axis column-tree moment connections with reduced beam section. Journal of Constructional Steel Research, 105, 28–38. https://doi.org/10.1016/j.jcsr.2014.10.005 Retrieved from http://dx.doi.org/10.1016/j.jcsr.2014.10.005

Ohsaki, M., Tagawa, H., & Pan, P. (2009). Shape optimization of reduced beam section under cyclic loads. Journal of Constructional Steel Research, 65(7), 1511–1519. https://doi.org/10.1016/j.jcsr.2009.03.001 Retrieved from https://linkinghub.elsevier.com/retrieve/pii/S0143974X09000558

Pachoumis, D. T., Galoussis, E. G., Kalfas, C. N., & Efthimiou, I. Z. (2010). Cyclic performance of steel moment-resisting connections with reduced beam sections - experimental analysis and finite element model simulation. Engineering Structures, 32(9), 2683–2692. https://doi.org/10.1016/j.engstruct.2010.04.038 Retrieved from http://dx.doi.org/10.1016/j.engstruct.2010.04.038

Rahnavard, R., Hassanipour, A., & Siahpolo, N. (2015). Analytical study on new types of reduced beam section moment connections affecting cyclic behavior. Case Studies in Structural Engineering, 3, 33–51. https://doi.org/10.1016/j.csse.2015.03.001 Retrieved from http://dx.doi.org/10.1016/j.csse.2015.03.001

Sofias, C. E., Kalfas, C. N., & Pachoumis, D. T. (2014). Experimental and FEM analysis of reduced beam section moment endplate connections under cyclic loading. Engineering Structures, 59, 320–329. https://doi.org/10.1016/j.engstruct.2013.11.010 Retrieved from http://dx.doi.org/10.1016/j.engstruct.2013.11.010

Swati, A. K., & Gaurang, V. (2014). Study of steel moment connection with and without reduced beam section. Case Studies in Structural Engineering, 1(1), 26–31. https://doi.org/10.1016/j.csse.2014.04.001 Retrieved from https://linkinghub.elsevier.com/retrieve/pii/S2214399814000058

Tezer, Ö. (2005). Reduced beam section beam-column connections. Turkey Engineering News, 54–59.